1 **Autonomous underwater vehicle based marine multi-component self-potential**

2 **method: observation scheme and navigational correction**

3

4 Zhongmin Zhu[1], Jinsong Shen[1], Chunhui Tao[2][3], Xianming Deng[2], Tao Wu[2], Zuofu Nie[1], Wenyi

5 Wang[1], Zhaoyang Su[1].

6 [1]State Key Laboratory of Petroleum Resources and Prospecting, China University of Petroleum

7 (Beijing), Beijing, 102249, China

8 [2]Second Institute of Oceanography, Ministry of Natural Resources, Hangzhou 310012, Zhejiang,

9 China

10 [3] School of Oceanography, Shanghai Jiaotong University, Shanghai 200030, China

11

12 **Corresponding author:** Jinsong Shen (shenjinsongcup@163.com)

13

14 Abstract

15 Marine self-potential (SP) investigation is an effective method to study deep-sea hydrothermal vents

16 and seafloor sulfide deposits. At present, the commonly used marine self-potential instrument is a

17 towed electrode array, large noise involves when the seafloor topography is complex, causing the

18 greatly change of electrode distance and array attitude. In this paper, a new multi-component electric

19 field observation system based on underwater autonomous underwater vehicle (AUV) was introduced

20 for the measurement of seafloor self-potential. The system was tested in a lake and the multi-

21 component self-potential data were collected. Observed data involve the navigational information of

22 AUV, which could be corrected using a rotation transform. After navigational correction, measured

23 data can recover the location of the artificial source well using self-potential tomography. The

24   experimental results showed that the new SP system can be applied to marine SP observations,

25   providing an efficient and low-noise SP acquisition method for marine resources and environmental

26   investigations.

27   **Keywords:** Underwater self-potential method; Autonomous underwater vehicles; Rotation correction;

28   Multi-component inversion;

29

30   Introduction

31   Self-potential (SP) method has a long history on land and plays an important role in the delineation

32   and resource evaluation of metal sulfide ore bodies (Fox, 1815). It is generally believed that the

33   negative anomaly of SP is related to the metal sulfide ore bodies (Sato and Mooney, 1960; Corry, 1985;

34   Naudet and Revil, 2005; Komori et al., 2017). In view of the great difference between the marine and

35   the terrestrial environments, economical and efficient geophysical exploration methods are still

36   missing, which limits the exploration and utilization of marine resources. With the development of

37   electronic instruments as well as better understanding of the mechanism of SP response, the application

38   of SP exploration has been gradually developed from land prospecting to shallow water and deep-sea

39   exploration of polymetallic sulfide (Corwin, 1973; Corwin, 1976; Tao et al., 2013). In addition to

40   mineral exploration, the underground water flow driven by seafloor thermal activity and thermal

41   gradient will also produce detectable SP anomalies. SP measurement method has also been applied to

42   study the geothermal and hydrothermal activity of deep seafloor (Heinson, 1999). Eppelbaum

43   （Eppelbaum, 2019）introduces a new parameter into SP interpretation -'self-potential moment', and

44   this method has been effectively applied at several ore deposits in the South Caucasus.

45   In 1973, Corwin (Corwin, 1973) began to develop the marine SP detection system, and in 1976, about

46   300 mV SP anomaly was discovered which related with the offshore extensions of sulfide deposit

47   (Corwin, 1976). In 2000, Sudarikov and Roumiantsev conducted SP and Eh (oxidation reduction

48   potential) survey at Logatchev hydrothermal vent in Mid-Atlantic ridge, and inferred the spatial

49   distribution characteristics of hydrothermal plume near the vent (Sudarikov and Roumiantsev, 2000).

50   Cherkashev (Cherkashev et al., 2013) used a deep-towed SP instrument to locate seafloor sulfide

51   deposits associated with hydrothermal vents near the mid-Atlantic ridge. Kawada and Kasaya (Kawada

52   and Kasaya, 2017, 2018) also observed negative SP anomalies and associated hydrothermal sulfide

53   deposits in the Izena hydrothermal field of the Okinawa trough in Japan by using the deep-sea towed

54   SP array. Safipour (Safipour et al., 2017) mounted SP electrodes on transient electromagnetic

55   equipment and detected SP negative anomaly over inactive sulfide at Tyrrhenian Sea.

56   The configuration described above connects the electrode array by a cable or insulated elastic rod,

57   which is easy to operate in marine environment. However, there are also several inconveniences with

58   soft-connected towed SP arrays. The towed array is susceptible to be distorted by ocean currents, and

59   the distance between the soft-connected electrodes changes greatly, both of which will affect the

60   precision of the measured SP amplitude, especially in the mid-ocean ridge area, where the seafloor

61   topography varies greatly (Constable et al., 2018).

62   To improve the stability and efficiency of marine SP configuration used in the deep-sea environment,

63   combined with the ideas of Constable et al. (2018), the autonomous underwater vehicle (AUV) was

64   modified with four electric field receivers in the tail to detect the marine SP responses (shorted, AUV-

65   SP), which was expected to be helpful for seafloor sulfide exploration. To test the stability and

66   determine the influencing factors, two dive AUV experiments were conducted during the July of 2019

67   at Qiandao Lake in eastern China. The water depth is about 40 m, and there was little human

68   interference around the test site, making it an ideal place to test the new system and analyze the electric

69   field noise. The main purpose of the AUV-SP system test was: i) to investigate the optimized position

70   of SP electrode on AUV to minimize the interference of running noise of AUV body to SP measurement;

71   ii) to verify the validation of developed system by using the known artificial current source. In addition,

72   measured multi-component data were inverted using self-potential tomography (Jardani et al., 2008;

73   Revil et al., 2008; Rittgers et al., 2013) to verify the capability of multicomponent self-potential

74   detection based on electrical field records.

75

76   ## 1. AUV-based SP system

77   SP measurement system mainly consisted of two parts, i.e. electric field receivers (Ag-AgCl non-

78   polarizing electrodes) and data logger chamber. The electronic circuit of the data logger was

79   encapsulated in the pressure chamber, which was mounted on the back of the AUV with a diving

80   capacity of 4500 m. The electric field receivers and two orthogonal extension rods of 2 m were

81   arranged horizontally and vertically at the tail of AUV (Figure. 1). The 1-channel and 2-channel

82   electrodes were fixed at the end of the horizontal extension rod along the running direction of AUV to

83   measure inline component of the electric field E_R. The 5-channel and 6-channel electrodes were

84   attached on the end of vertical extension rod to measure the vertical component E_V. The 3-channel and

85   4-channel electrodes were mounted on the left and right sides of the abdomen of AUV to measure the

86   horizontal component orthogonal to the AUV E_T. The E_T data for electrodes on surface of AUV were

87   affected by propulsion motor and short electrode space (less than 30cm), leading a larger noise level

88   than the rear electrodes. The component E_T were greatly distorted; thus, the followed data processing

89   and analysis would focus on the E_R and E_V.

90   The installation of the SP receivers did not affect the data flow or function of other sensors mounted

91   on AUV including magnetic field sensor, sonar to avoid obstacles, underwater cameras and other

92   plume detective sensors. Navigational parameters including the vehicle's positions with an ultra-short

93   baseline, pressure depths and attitude orientation (Wu et al., 2019).

94

95   ## 2. Lake test design and data acquisition of AUV based SP system

96   *2.1 Noise levels and observation design*

97   There are different disturbances appearing in the SP method, including natural noise and artificial noise

98   (Eppelbaum, 2020). The electrode is calibrated in the laboratory., and the potential difference between

99   the electrode pairs is less than 0.1 mv. Therefore, the main factors affecting the SP signal strength and

100   quality on AUV were as follows: electrode spacing, the stability of the observation system and the

101   interference to the electrodes from the AUV body (batteries, thrusters, etc.). The signal of natural

102   electric field in deep seawater was very weak, and the measured magnitude of electric potential

103   difference was in direct proportion to the electrode distance. Large electrode distance should be used

104   for weak signal, and the electrode distance should be increased as much as possible without affecting

105   the normal navigation of AUV. The electrode distance in the lake test was preset as 2 m.

106   Considering the interference of the electrode by the AUV power supply device, a pair of electrodes

107   were placed on the surface of the AUV, and the other two groups of electrodes were installed at the tail

108   of the AUV with the hard-connecting rod as a bracket, as far as possible away from the AUV body.

109   The reason for choosing the hard-connecting rod was to keep the electrode distance constant when the

110   submersible moves underwater. It is very important in the marine SP detection. The soft link rod will

111   be distorted by bottom current of seawater when AUV moves near the seafloor and therefore would

112 not be suitable. Changing of electrode distance will introduce the attitude deformation noise and

113 strongly affect the recorded signals especially when the electrode distance is small.

114 *2.2 Equipments used for the test*

115 As the materials of hard-connecting rod to connect the electrodes, on the one hand, non-magnetic

116 materials should be used to minimize the influence on the fluxgate magnetometer at the tail of the

117 submersible. On the other hand, the connecting rod should be insulated to electric current to minimize

118 the induced electric field generated by cutting the earth magnetic field during the movement of AUV.

119 The electrode bracket used in the lake test was made of PVC material without magnetic components

120 and fully insulated. These conditions meet the above requirements.

121 *2.3 Layout of artificial SP source*

122 The test of the AUV based SP system was conducted at a testing platform, in the center of Qiandao

123 Lake. According to the classic geo-battery model (Sato and Mooney, 1960), SP anomalies generated

124 by the geo-battery mechanism are expected to be dipolar in nature and the SP source can be equivalent

125 to electric dipole source (see also Naudet and Revil, 2005, for biogeobatteries). To verify the

126 effectiveness of AUV-SP system, an artificial diploe source was set up as shown in Figure. 2. Firstly,

127 a 100 m nylon rope was mounted on an insulating float for fixing test platform, and four buoys were

128 mounted in the middle of rope to make it float on the surface of the water. Positive and negative

129 electrodes were extended by wires, which were fixed along the rope into the lake. The distance between

130 the positive and negative poles was about 56 m. The 36 V DC power supply was placed in the platform.

131 The copper plates were mounted in the positive and negative terminals, respectively, to reduce the

132 voltage attenuation and increase the conductive area of the current electrode.

133 *2.4 Data acquisition*

134 Before the AUV entered the water, all electrodes were placed on the AUV system as shown in Figure.

135 1. AUV firstly dived to 8 m depth at a constant speed, and performed repeated measurements

136 surrounding the positive and negative poles. The average speed of the AUV was about 1 knot (0.5 m/s),

137 and the sampling frequency of the electric field sensor was 150 Hz. Other tests including repeatedly

138 switching on and off manual power, changing navigation speed and steering were also conducted to

139 determine the influence of AUV body on the electric field signal during navigation.

140

141 3. Results and analysis

142 *3.1 Noise analysis of the lake test*

143 Figure 3 shows the three-component electric field in water. The artificial source produced a stable

144 electric field similar to an electric dipole source in water. At the beginning of entering water, the system

145 was far away from the negative pole, and the collected electric field was approximately equal to the

146 background field. The amplitude fluctuated around 0 mV. When passing near the location of the

147 artificial current source, the electric field sensor could detect that the potential changed up to 30 mV.

148 Because the system was always close to the negative electrode during the measurement process, the

149 recorded electrical field was less affected by the positive pole/electrode.

150 In order to analyze the influence of AUV body on the electric field sensor, the frequency spectrum of

151 the electric field time series measured by the artificial current source was analyzed. Figure. 4 shows

152 the time series data of the three-component electric field for 15 min. The overall noise level was related

153 to the position of the electrode. Results of spectrum calculation showed the following characteristics:

154 1)   The effective signal was mainly concentrated in the low frequency, and the noise level decreased

155   with the increase of frequency;

156   2)   The electrode far from the AUV body demonstrated lower noise;

157   3)   The noise of vertical component was lower than that of horizontal one;

158   4)   Except for the 50 Hz industrial interference, the peak values of the power spectrum were basically

159   consistent with the rotation speed of propellers.

160   In addition, the noise of 2.1 Hz corresponding to the vertical component was mainly caused by the

161   vibration of the connecting rod in the water. The camera attached to the head of the connecting rod

162   recorded the corresponding vibration image, providing a reference for improving the material and

163   installation mode of the connecting rod.

164   *3.2 AUV navigation attitude impact and correction*

165   The attitude of AUV has a significant influence on the SP data, so the attitude change should be

166   considered and corrected in the field data processing and interpretation. The attitude angle in the local

167   coordinate system is usually used to describe the attitude and spatial position of AUV, including

168   azimuth angle (heading), pitch angle and roll angle. The global reference coordinate system was

169   determined according to the geodetic coordinates and the position of the survey lines. Then the relative

170   relationship between the two coordinates was determined by the rotation of the coordinate system as

171   shown in Fig. 5c. The coordinate axis of the reference coordinate system is assumed as (X_0, Y_0, Z_0).

172   The local coordinate system of the first rotation (X_1, Y_1, Z_1) is obtained by rotating the azimuth angle

173   H clockwise with Z_0 as the rotation axis, then (X_2, Y_2, Z_2) is obtained by rotating pitch angle P

174   clockwise respect with X_1, and finally (X_3, Y_3, Z_3) is obtained by rotating the roll angle R

175   clockwise along Y_2 axis. The above procedure can be represented by three rotation matrices below.

176   The electric field supposed to be rotated in the reference coordinate system is $\mathbf{E}_g(E_x, E_y, E_z)$, and the

177   measured electric field in the local coordinate system after rotation is $\mathbf{E}_{rot}(E_R, E_T, E_V)$, then

178   $E_{rot} = RY \cdot RX \cdot RZ \cdot E_g$ is written as the component form:

179
$$\begin{bmatrix} E_R \\ E_T \\ E_V \end{bmatrix} = \begin{bmatrix} \cos R & 0 & -\sin R \\ 0 & 1 & 0 \\ \sin R & 0 & \cos R \end{bmatrix} \begin{bmatrix} 1 & 0 & 0 \\ 0 & \cos P & \sin P \\ 0 & -\sin P & \cos P \end{bmatrix} \begin{bmatrix} \cos H & \sin H & 0 \\ -\sin H & \cos H & 0 \\ 0 & 0 & 1 \end{bmatrix} \begin{bmatrix} E_x \\ E_y \\ E_z \end{bmatrix} \quad (1)$$

180   The corresponding inverse transformation is:

181
$$E_g = (RY \cdot RX \cdot RZ)^{-1} E_{rot} = RX^T \cdot RZ^T \cdot RY^T E_{rot} \qquad (2)$$

182   The AUV will take such operations as obstacle avoidance and steering according to the change of

183   submarine terrain when flying over seafloor. The electric field $\mathbf{E}_{obs}$ recorded by the sensors attached

184   to the AUV contains information about the navigation attitude. By ignoring acquisition noise and

185   positioning error, $\mathbf{E}_{obs}$ recorded by AUV should be consistent with the rotated $\mathbf{E}_{rot}$. It can be verified

186   whether the measured electric field of AUV is consistent with the electric field generated by dipoles

187   in uniform space through numerical simulation.

188   According to the situation of the lake test, a three-dimensional (3D) model of 100×100×30 m was

189   established in Cartesian coordinate system, where positive and negative poles of the dipole were

190   located at (3, 75, -1) and (54, 80, -0.5), respectively. The 3D model was discretized into unstructured

191   grids; the Poisson equation of steady-state current field was solved by the finite element method; and

192   boundary conditions of the first kind were used at the bottom of the lake. The global electric field

193   $\mathbf{E}_g(E_x, E_y, E_z)$ was extracted according to AUV location data, and then the electric field in the local

194   coordinate system along the direction of profile denoted as $\mathbf{E}_{rot}(E_R, E_T, E_V)$ was calculated using

195   Eq.(1). Field data measured by the AUV were denoted as $\mathbf{E}_{obs}(E_R, E_T, E_V)$. The relationship between

196   global $\mathbf{E}_g(E_x, E_y, E_z)$ and local $\mathbf{E}_{rot}(E_R, E_T, E_V)$ is shown in Fig. 5b. When AUV is moving north,

197   the observation field is in the same direction as the reference field, and opposite as AUV moving from

198   north to south.

199   The attitude of AUV is shown in Fig. 6a. AUV flew stable in the lake and the roll angle was less than

200   5°. Pitch changed when vehicle was rising or falling and the overall pitching angle was less than 20°.

201   In the measured range shown in Fig. 6a, the vehicle changed direction twice at 02:11 and 02:14,

202   respectively. The measured and simulation results in Fig. 6b and Fig. 6c showed that the attitude of the

203   submersible has different impacts on each component of the electric field. Specifically, the azimuth

204   has significant influence on the horizontal component of the electric field, but has little influence on

205   the vertical component. When the survey line went along SW, variation trend of $\mathbf{E}_R$ along the survey

206   line (red solid line in Fi. 6b) and global component $\mathbf{E}_x$ was in the opposite; when the survey line went

207   along northeast (NE), $\mathbf{E}_R$ and $\mathbf{E}_x$ changed in the same direction. After rotation correction, the

208   observation data of the submersible were basically consistent with the simulation results. The position

209   where the gradient of the horizontal electric field component changed the most significantly,

210   corresponded to the negative pole of the artificial source. Azimuth has little effect on the vertical

211   component, because the submersible is always below the negative source and the electric field

212   direction always points up. Therefore, the change of azimuth angle will not change the direction of the

213   vertical component. In addition, because that the pitch angle was very small, and the attached electrode

214   was basically maintained in the vertical state, the vertical component of the measured electric field

215    $\mathbf{E}_V$ was approximately equal to that of the global component $\mathbf{E}_Z$.

216

217   ## 4. Inversion Scheme of AUV based self-potential data

218   The forward problem of SP can be expressed by Poisson equation of potential (Jardani et al.,2008):

219
$$\nabla \cdot (\sigma \nabla V) = \nabla \cdot \mathbf{J}_s = \Im$$
$$\mathbf{E} = -\nabla V$$
    (3)

Geoscientific
Instrumentation
Methods and
Data Systems

Discussions

220   where $\Im$ is the volumetric current density (A/m³), $\mathbf{J}_s$ is the current density vector (A / m²), σ is the

221   conductivity (S/m), $\mathbf{E}$ is the electric field vector, and V represents the SP field.

222   By changing the source term of Eq. (3), the SP response to various effects can be calculated, such as

223   the flow potential related to groundwater flow (Ahmed et al., 2013) or the geo-battery model related

224   to polymetallic deposits (Rittgers et al., 2013).

225   In order to investigate the reliability and interpretability of electric field data measured by the AUV-

226   SP system, the regularized least square method was applied for the inversion of the artificial SP source.

227   Assuming that m is the bulk current density model vector and m_0 is the reference model, the

228   inversion can be expressed as the minimization of the following objective function：

229    $$\phi(m) = \left\| \mathbf{W_d} \Delta d \right\|^2 + \alpha \left\| \mathbf{W}(m - m_0) \right\|^2 \qquad (4)$$

230   where $\mathbf{W_d}$ is the data weighting matrix, Δd is the difference between the data d obtained by forward

231   modeling and the observed data d^{obs}, that is data residual. Here, the measured electric field

232   component was selected as the observation data, $\mathbf{W}$ is the model weighted diagonal matrix, and α as

233   the regularization factor. Regularization factor α was used to balance the model constraints and data

234   fitting function in the process of solving the model. It can be determined by L-curve criterion or GCV

235   method, or by experience. Because the electric field decays rapidly with distance, the inversion of

236   seafloor SP data only gives a shallow current density distribution, which cannot accurately reflect the

237   situation of space current dipole source under the seafloor. Therefore, it is necessary to introduce depth

238   weighting function to enhance the sensitivity of grid element far from the observation point. The depth

239   weighting function $\mathbf{W_z}$ should be placed in the model constraints as follows (Biswas and Sharma,

240   2017; Portniaguine and Zhdanov, 1999):

241    $$W_j = \left(\sum_{i=1}^{N} (J_{ij})^2 \right)^{p/4}, \ j = 1, ..., M \qquad (5)$$

242   where W_j is the jth element on the main diagonal of matrix $\mathbf{W_z}$, $\mathbf{J}$ is the sensitivity matrix (or

243   Jacobian matrix) calculated using forward. M is the number of model vector elements; N is the number

244   of the observation point. p is constant, generally equal to 1. The extent of depth weighting can be

245   adjusted by the value of p. For multi-component inversion, the full three electric field are used and the

246   total number of observation data becomes 3*N.

247   In application, the SP data can be inverted in many ways to determine the flow direction of the fluid

248   or the location of the self-potential source. When the source location is to be solved, it was usually

249   assumed that the conductivity distribution in the space is known or determined by other electrical

250   exploration methods (DC conductivity or induction-based electromagnetic methods), then the SP

251   source can be equivalent to the external current source. Therefore, this study used the inverted

252   volumetric current density distribution to locate the simulated artificial source. On land, SP method

253   usually directly measures the electric potential between the roll electrode and a fixed electrode,

254   therefore, the potential data V is directly chosen for inversion. However, in the marine environment, it

255   is impossible to fix a reference electrode on the seafloor when the ship or AUV is moving. Therefore,

256   the SP method conducted in the marine environment usually measures the gradient of electric potential,

257   that is the electric field, and the potential is calculated indirectly by numerical integration. In the case

258   of this study, the measured multi-components electric field components were directly inverted.

259   Owing to the observation data collected by AUV-SP system near the artificial source are limited, the

260   inversion result is nonunique. Therefore, the constraints of known information such as the lake water

261   conductivity (1 S/m, measured with the environment sensor from AUV) and lake bottom sediment

262   conductivity (assumed as 0.1 S/m) were added to the inversion. To investigate the advantages of multi-

263   component inversion, single component and two component observation data were used for inversion

264 and the inversion results were compared. Figure 7. shows the results obtained by inversion of electric

265 field data of single component (horizontal component, vertical component, respectively) and two

266 components (horizontal component and vertical component) under the same constraint conditions.

267 Negative charge density was recovered surrounding the negative pole of the artificial source in all

268 results, which preliminarily revealed the reliability of the system and the effectiveness of the inversion

269 method. Indeed, cause the AUV-SP system's navigation path in the lake is mainly near the negative

270 pole of the artificial source, the negative pole position of the artificial source can be precisely located

271 while positive pole is not well-located cause lack of observation data of surrounding area, although

272 some positive charge density is retrieved along the survey line. By comparing the inversion results

273 between single component (Figure.7a and b) and multi-component (Figure.7c), it was observed that

274 the inversion results of the two horizontal components of the electric field were more focused, and the

275 negative charge intensity was concentrated, while the negative charge density obtained from the

276 inversion results of the single vertical component of the electric field was accompanied by positive

277 charge anomaly, which dispersed the negative charge energy, and deviated from the actual situation.

278 Combination of vertical and horizontal components of electric field data restricts the horizontal

279 distribution of charge density and makes the inversion more consistent with the actual artificial source.

280 In addition, the current flow direction (Figure. 7b, d, f) also exhibits that the inversion of only one

281 single component will produce wrong current direction, more additional constraints (e.g. boundary

282 limits, heterogeneous distribution of conductivity) were required to obtain reasonable inversion results.

283 Therefore, multi-component detection of electric field is necessary when address complex geological

284 structure especially involving flow patten of fluids.

285

5. Conclusion

286

287 A seafloor SP measurement system which consisted of three pairs of perpendicular electric field

288 receivers attached to the AUV (Qianlong 2) was introduced. By introducing an artificial current source,

289 the multi -component electric field responses in the water were measured by AUV in Qiandao Lake.

290 The observed results were consistent with the numerical simulation, which verifies the feasibility of

291 the AUV-SP system for multi-component SP exploration. At present, the AUV-SP system can work in

292 water for about 40 hours, and complete the SP measurement of high-resolution area of about 20 km^2.

293 The test results of two surveys showed that the AUV-SP system has good consistency and repeatability,

294 and the overall noise level of the measured data is relatively low, which basically meets the

295 requirements of near seafloor SP exploration in large scale. The inversion of the test data of AUV-SP

296 system demonstrated that the position and intensity of the inverted current source were basically

297 consistent with the actual position and intensity of the artificial current source. Therefore, the SP

298 response measured by AUV-SP system can be used to locate the seafloor SP source, so as to achieve

299 the exploration and evaluation of the seafloor sulfide deposits. In the case of simple geoelectric

300 structure, single vertical component measurement would be sufficient to locate the SP source, but in

301 solving the complex problems such as hydrothermal or fluid flow, three-component SP measurement

302 is necessary.

303 In view of the vibration noise of the connecting rod presented in this test, our next step will be to select

304 a more suitable material and design a bracket with better rigidity to reduce the vibration noise. The

305 experience and data accumulated in this experiment also provide a reference for the future researches

306 of active source electromagnetic detector on AUV.

307 ***Data availability***

308   The raw data from the experiments are available upon request (591149254@qq.com)

309   ***Author contributions***

310   ZZ process the data and wrote the paper. JS was the project leader. CT provided ideas and designed

311   the AUV-SP system, XD, TW, ZN and WW together test the system, ZS proofread the manuscript.

312   *Competing interests*

313   The authors declare that they have no conflict of interest.

314   *Acknowledgements*

317   ***Financial support***

321

References:

Ahmed, A. S., Jardani, A., Revil, A., and Dupont, J. P.: SP2DINV: A 2D forward and inverse code for streaming potential problems. Computers & Geosciences, 59, 9-16, https://doi.org/10.1016/j.cageo.2013.05.008, 2013.

Biswas, A., and Sharma, S. P.: Interpretation of self-potential anomaly over 2-D inclined thick sheet structures and analysis of uncertainty using very fast simulated annealing global optimization, Acta Geodaetica et Geophysica, 52, 439-455, https://doi.org/10.1007/s40328-016-0176-2, 2017.

Cherkashev, G. A., Ivanov, V. N., Bel Tenev, V. I., Lazareva, L. I.,Rozhdestvenskaya, I. I., Samovarov, M. L., Poroshina, I. M., Sergeev, M. B., Stepanova, T. V., and Dobretsova, I. G.,: Massive sulfide ores of the northern equatorial Mid-Atlantic Ridge, Oceanology, 53, 607-619, https://doi.org/10.1134/S0001437013050032, 2013.

Constable, S., Kowalczyk, P., and Bloomer, S., Measuring marine self-potential using an autonomous underwater vehicle, Geophysical Journal International, 215, 49-60, https://doi.org/10.1093/gji/ggy263, 2018.

Corry, C. E.,: Spontaneous polarization associated with porphyry sulfide mineralization, Geophysics, 50, 1020-1034, https://doi.org/10.1190/1.1441967, 1985.

Corwin, R. F.: Offshore Application of Self-potential Prospecting, Scripps Institution of Oceanography Library, 1973.

Corwin, R. F.: Offshore use of the self-potential method: Geophysical Prospecting, 24, 79-90, https://doi.org/10.1111/j.1365-2478.1976.tb00386.x, 1976.

Eppelbaum, L.V.: Advanced analysis of self-potential field analysis in ore deposits of the South Caucasus, Proceedings of the National Azerbaijan Academy of Sciences, 2, 21-35, DOI: 10.33677/ggianas20190200029, 2019.

Eppelbaum, L. V.: Quantitative analysis of self-potential anomalies in archaeological sites of Israel: an overview. Environmental Earth Sciences, 79, 1-15, https://doi.org/10.1007/s12665-020-09117-w, 2020.

Fox R W.: On the electro-magnetic properties of metalliferous veins in the mines of cornwall. Abstracts of the Papers Printed in the Philosophical Transactions of the Royal Society of London. London, 411-411. 1833

351 Heinson, G.: Marine self potential exploration: Exploration Geophysics, 30, 1-4,
352   https://doi.org/10.1071/EG999001, 1999.

353 Jardani, A., Revil, A., Bolève, A. and Dupont, J. P.: Three-dimensional inversion of self-potential data
354   used to constrain the pattern of groundwater flow in geothermal fields, Journal of Geophysical
355   Research, 113, B09204, https://doi.org/10.1029/2007JB005302, 2008.

356 Kawada Y, Kasaya T. Marine self-potential survey for exploring seafloor hydrothermal ore deposits.
357   Scientific reports, 7(1), 1-12. https://doi.org/10.1038/s41598-017-13920-0, 2017

358 Kawada, Y., and Kasaya, T.: Self-potential mapping using an autonomous underwater vehicle for the
359   Sunrise deposit, Izu-Ogasawara arc, southern Japan, Earth, Planets and Space, 70, 142,
360   https://doi.org/10.1186/s40623-018-0913-6, 2018.

361 Komori, S., Masaki, Y., Tanikawa, W., Torimoto, J., Ohta, Y., Makio, M., Maeda, L., Ishibashi, J.,
362   Nozaki, T., Tadai, O., and Kumagai, H.: Depth profiles of resistivity and spectral IP for active
363   modern submarine hydrothermal deposits: a case study from the Iheya North Knoll and the Iheya
364   Minor Ridge in Okinawa Trough, Japan, Earth, Planets and Space, 69, 114
365   https://doi.org/10.1186/s40623-017-0691-6, 2017.

366 Naudet, V., and Revil, A.: A sandbox experiment to investigate bacteria-mediated redox processes
367   on self-potential signals, Geophysical Research Letters, 32, L11405,
368   https://doi.org/10.1029/2005GL022735, 2005.

369 Portniaguine, O., and Zhdanov, M. S.: Focusing geophysical inversion images, Geophysics, 64, 874-
370   887, https://doi.org/10.1190/1.1444596, 1999.

371 Revil, A., Finizola, A., Piscitelli, S., Rizzo, E., Ricci, T., Crespy, A., Angeletti, B., Balasco, M., Barde
372   Cabusson, S., Bennati, L., Bolève, A., Byrdina, S., Carzaniga, N., Di Gangi, F., Morin, J., Perrone,
373   A., Rossi, M., Roulleau, E.,and Suski, B,: Inner structure of La Fossa di Vulcano (Vulcano Island,
374   southern Tyrrhenian Sea, Italy) revealed by high‐resolution electric resistivity tomography
375   coupled with self‐potential, temperature, and CO_2 diffuse degassing measurements, Journal of
376   Geophysical Research: Solid Earth, 113, B07207, https://doi.org/10.1029/2007JB005394, 2008.

377 Rittgers, J. B., Revil, A., Karaoulis, M., Mooney, M. A., Slater, L. D., and Atekwana, E. A.: Self-
378   potential signals generated by the corrosion of buried metallic objects with application to
379   contaminant plumes, Geophysics, 78, EN65-EN82, https://doi.org/10.1190/geo2013-0033.1,

380   2013.

381   Safipour, R., Hölz, S., Halbach, J., Jegen, M., Petersen, S., and Swidinsky, A.: A self-potential

382   investigation of submarine massive sulfides, Palinuro Seamount, Tyrrhenian Sea, Geophysics,

383   82(6), A51-A56, https://doi.org/10.1190/geo2017-0237.1, 2017.

384   Sato, M., and Mooney, H. M.: The electrochemical mechanism of sulfide self-potentials, Geophysics,

385   25, 226-249, https://doi.org/10.1190/1.1438689, 1960.

386   Sudarikov, S. M., and Roumiantsev, A. B.: Structure of hydrothermal plumes at the Logatchev vent

387   field, 14 45′ N, Mid-Atlantic Ridge: evidence from geochemical and geophysical data, Journal

388   of Volcanology and Geothermal Research, 101, 245-252, https://doi.org/10.1016/S0377-

389   0273(00)00174-8, 2000.

390   Tao, C., Xiong, W., Xi, Z., Deng, X., and Xu, Y.: TEM investigations of South Atlantic Ridge 13.2 S

391   hydrothermal area, Acta Oceanologica Sinica, 32, 68-74, https://doi.org/10.1007/s13131-013-

392   0392-3, 2013.

393   Wu, T., Tao, C., Zhang, J., Wang, A., Zhang, G., Zhou, J., and Deng, X.: A hydrothermal investigation

394   system for the Qianlong-II autonomous underwater vehicle, Acta Oceanologica Sinica, 38, 159-
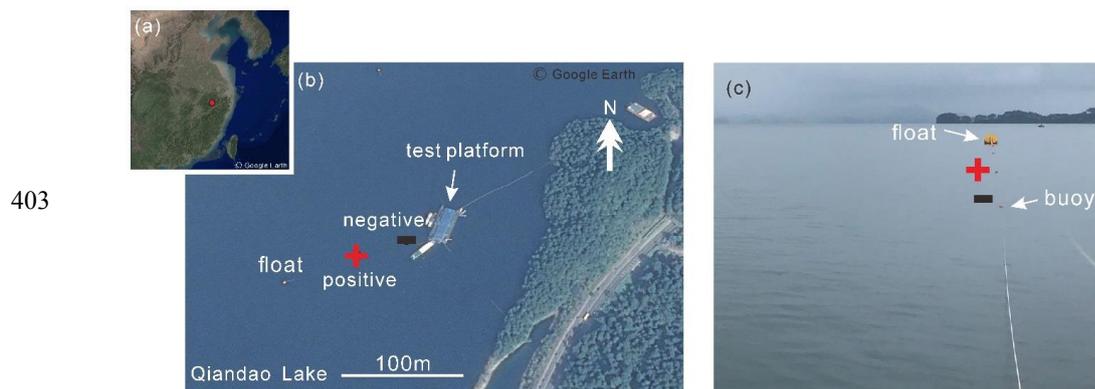
395   165, https://doi.org/10.1007/s13131-019-1408-4, 2019.

396
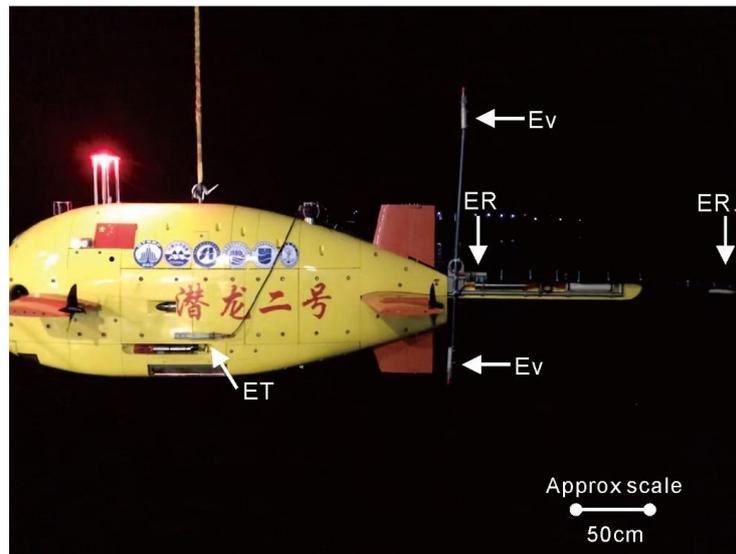
Figures


Figure.1. Layout of each channel electrode on AUV. E_R is the inline horizontal component of electric

field recorded by channel 1 and 2; E_T is the crossline horizontal component of electric field recorded

by channel 3 and 4; E_V is the vertical component of electric field recorded by channel 5 and 6.

403

404 **Figure.2.** Layout of artificial SP source. (a) Location of Qiandao Lake (source: Google Earth, 2019);

405 (b) Position of artificial source in the water (plan view) (source: Google Earth, 2019); (c) Zoom in

406 location of artificial source, red plus and black minus denote the positive and negative poles of the DC

407 power, respectively.

408

409
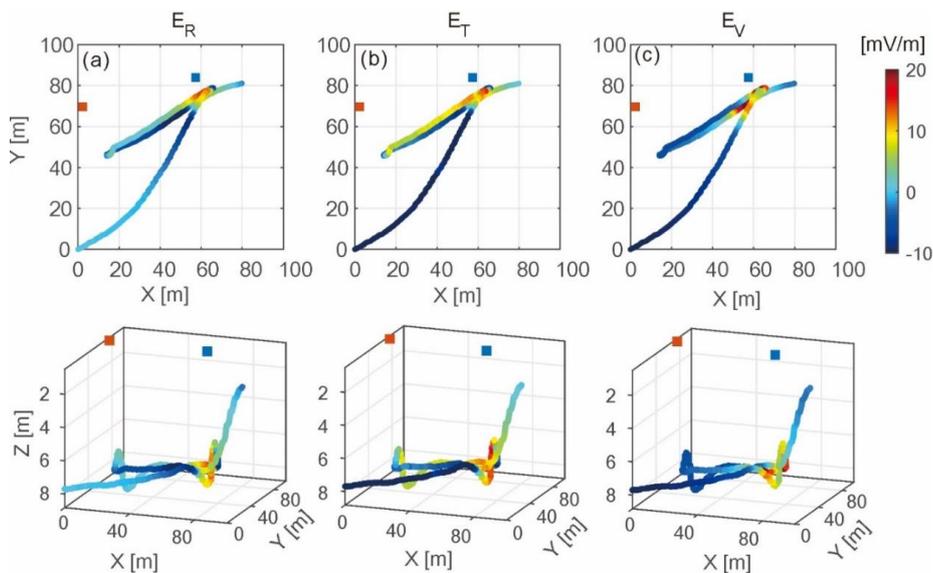
Figure.3. The planar distribution of the three components of the electric field measured by AUV based

SP system (plan view in the upper panel, 3D view in the lower panel). (a) Inline component of electric

field, (b) Crossline component of electric field, (c) Vertical component of electric field; Red and blue

dots represent the positive and negative poles of the artificial source, respectively.

414

415

416

417
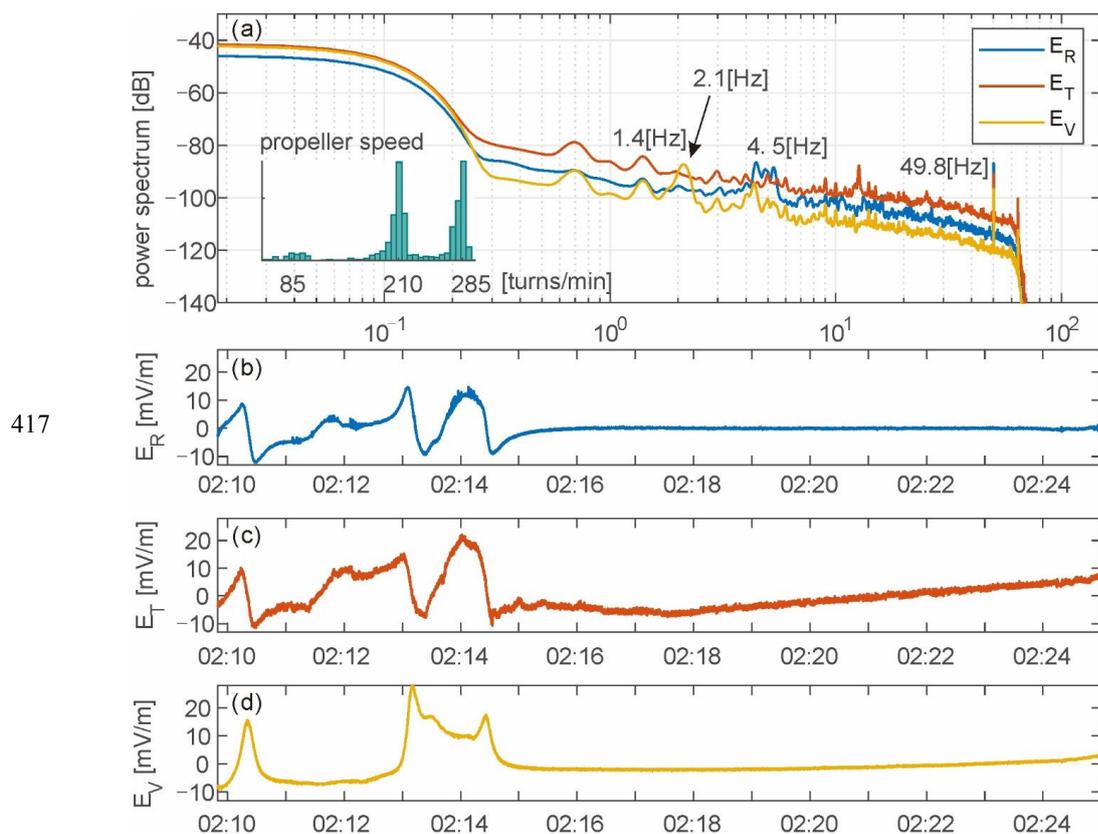
Figure.4. Time series of three components of electric field and frequency analysis of recorded data. (a)

Spectrum of three components of electric field with the histogram of propeller speed, (b) time series

of inline component E_R, (c) time series of crossline component E_T, and (d) time series of vertical

component E_V.

418

419

420

421

422
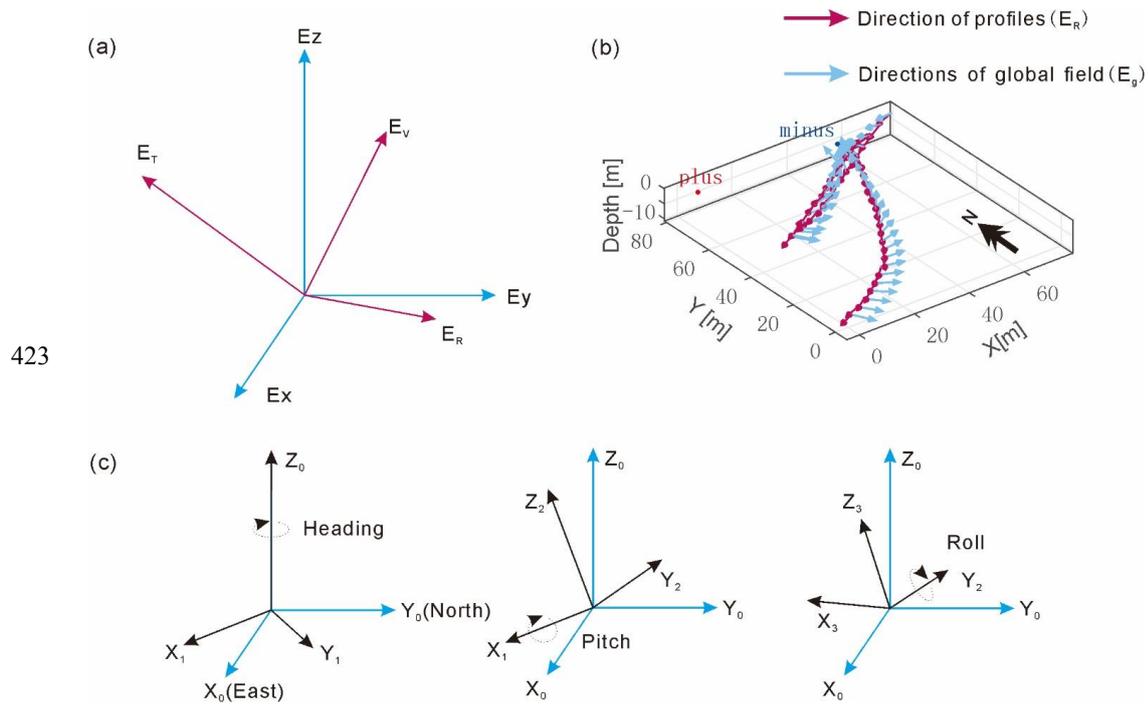
Figure.5. Rotation relationship between global electric field $\mathbf{E}_g$ and rotated electric field $\mathbf{E}_{rot}$. (a) The projection of the global and rotated electric fields in Cartesian coordinate system; (b) path of AUV in water, arrows denote the direction of AUV moving and vector direction of total electric field in geodetic coordinate system, plus denote the position of positive pole, minus denote the position of negative pole; (c) definition of different attitude angles.

430
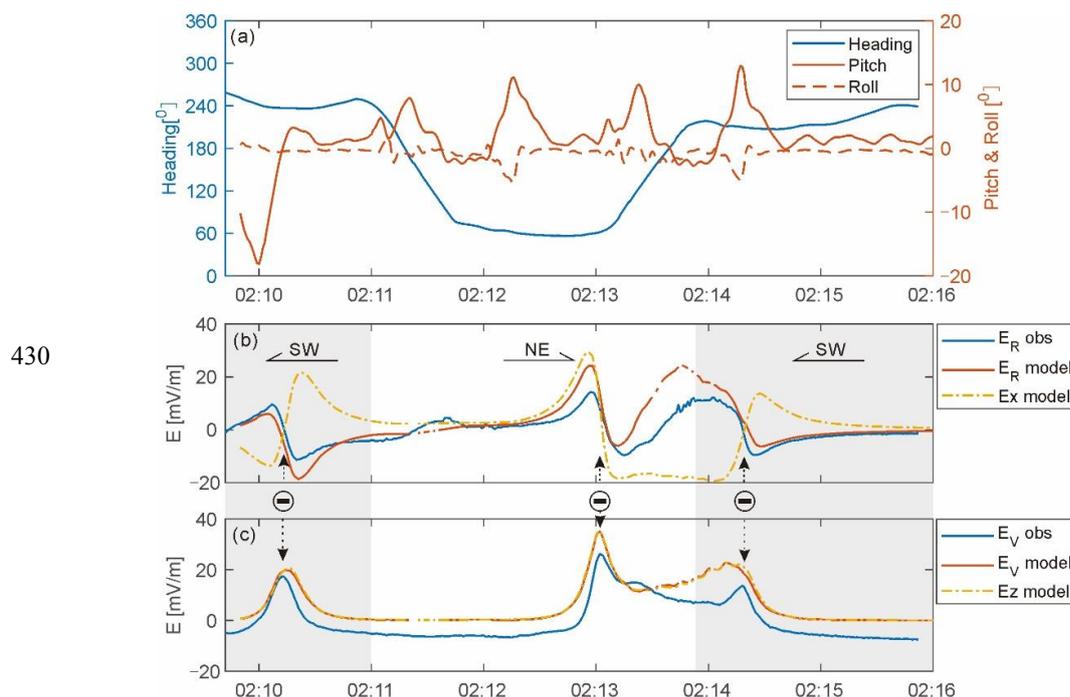
431 **Figure.6.** Comparison of the measured data and numerical simulation. (a) Navigation attitude of AUV

432 in the water; (b) time serious of modelling and observed horizontal component with different travel

433 direction; (c) modelling and observed vertical component for SW-NE-SW profiles. Minus corresponds

434 to the location of negative pole of the artificial source.

435
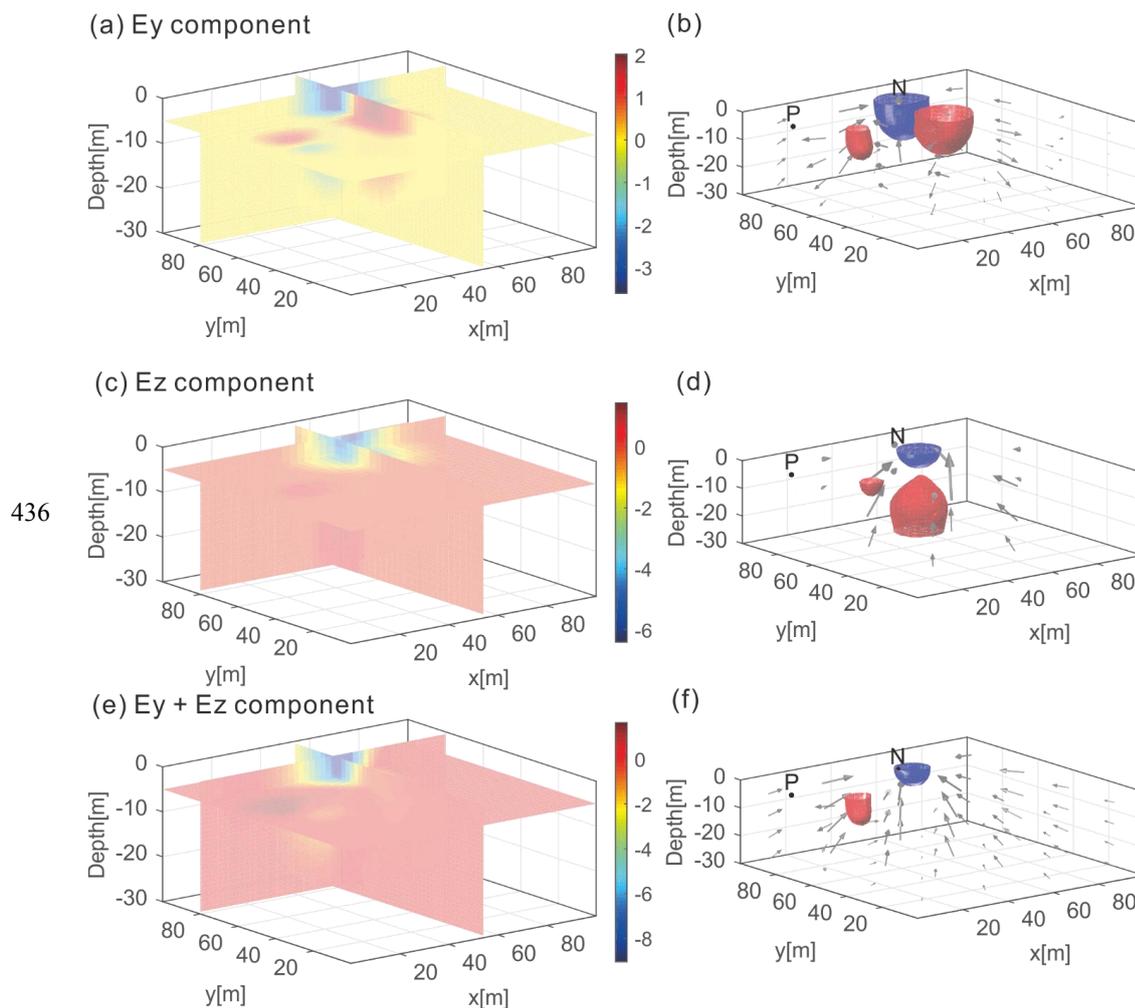
Figure.7. Volumetric current density inversion results of different components of observed data, with p = 1 and α=0.01 (a) and (b) Inversion results of volumetric current density of horizontal components of electric field data (magnitude and direction), (c) and (d) Inversion results of charge density of vertical component of observed data (magnitude and direction). (e) and (f) Inversion results of charge density of both two component of observed data (magnitude and direction). The arrow direction indicates the diffusion direction of the current density. The intersection of the vertical section is the position of the negative pole of the artificial source. Although the anomaly recovery for single component can also localize the negative pole, two component inversion returns a single and compact current density. The notation P corresponds to the location of positive pole of the artificial source. The notation N corresponds to the location of negative pole.